Analysis of nonlinear effects on ultrashort laser pulses in emerging optical fiber technologies

MOUNIR KHELLADI[1], DJELLOUL AISSAOUI[2], ABDELHALIM RABEHI[2], ABDELMALEK DOUARA[3], ABDELAZIZ RABEHI[2,*], MOHAMED BENGHANEM[4,*]
[1]*Telecommunication department, Faculty of Technology, University of Tlemcen, Tlemcen 13000, Algeria*
[2]*Laboratory of Telecommunication and Smart Systems (LTSS), Faculty of Science and Technology University of Djelfa, PO Box 3117, Djelfa 17000, Algeria;*
[3] *Faculty of Science and Technology, Tissemsilt university, Tissemsilt 38000, Algeria*
[4]*Physics Department, Faculty of Science, Islamic University of Madinah, Madinah, 42351, Saudi Arabia*

Ultrashort laser pulses, characterized by pulse durations in the picosecond to femtosecond range, present significant potential for enabling ultra-high data rate transmission in optical communication systems. Understanding the propagation of these pulses in nonlinear media is critical due to the complex effects they encounter, including chromatic dispersion and various nonlinear phenomena. The propagation of ultrashort laser pulses in optical fibers is governed by the generalized nonlinear Schrödinger equation (GNLSE), which incorporates effects such as self-phase modulation (SPM), cross-phase modulation (XPM), self-steepening (SS), and stimulated Raman scattering (SRS). This equation effectively models the interplay between dispersion and nonlinearity in various fiber structures, including silica fiber (SiO_2), air-silica, photonic crystal fibers (PCFs), and Air-filled core. Analysis reveals that air-silica outperforms conventional fibers in terms of pulse compression and peak power handling. Our simulations reveal compelling pulse dynamics: an initial 8 ps pulse undergoes width compression to 4.04 ps, while its peak power intensifies from 1.23 kW to 69 kW upon propagation. Their reduced dispersion and nonlinear interactions make them optimal candidates for high-fidelity ultrashort pulse transmission.

(Received August 7, 2025; accepted April 6, 2026)

Keywords: Ultrashort laser pulses, Nonlinear Schrödinger equation, Photonic crystal fiber, Hollow-core fiber, Dispersion, Nonlinear effects

1. Introduction

Ultrashort laser pulses are essential in modern optical communication and photonic applications due to their ability to support ultra-high-speed data transmission. Propagating such pulses in optical media involves complex interactions between dispersion and nonlinear effects, making their accurate modelling and analysis crucial. Recent advancements in optical fiber technologies, including photonic crystal fibers (PCFs) and hollow-core fibers, have enabled better control of these interactions. Traditional optical fibers, such as fused silica, suffer from high dispersion and nonlinear effects, which can significantly distort ultrashort pulses during transmission. In contrast, PCFs and hollow-core fibers offer improved confinement and reduced optical loss, making them promising candidates for advanced communication systems [1-3].

The main challenges in ultrashort pulse propagation arise from chromatic dispersion, which causes pulse broadening and temporal spreading; nonlinear effects including SPM, XPM, and SRS that alter pulse shape and spectral characteristics; and energy losses resulting from attenuation and inelastic scattering mechanisms such as Raman and Brillouin scattering.

The propagation characteristics of ultrashort pulses are governed by the nonlinear Schrödinger equation (GNLSE) [4-6], which describes the balance between dispersion and nonlinearity. For more complex scenarios, the generalized nonlinear Schrödinger equation (GNLSE) accounts for higher-order effects such as self-steepening and stimulated Raman scattering. These effects play a significant role when ultrashort pulses propagate through nonlinear optical media, and understanding their influence is critical for optimizing pulse transmission.

Among the different optical media available, photonic crystal fibers and hollow-core fibers present unique properties that distinguish them from conventional fused silica fibers [7-8]. Photonic crystal fibers utilize a periodic microstructure to guide light and can achieve highly controlled dispersion and confinement. Hollow-core fibers, however, guide light through an air-filled core, significantly reducing material interactions and minimizing dispersion and nonlinear effects. These unique properties make them attractive for applications requiring precise control over ultrashort pulse propagation.

Ultrashort laser pulses have numerous applications beyond optical communications. They are used in spectroscopy, biomedical imaging, material processing, and ultrafast science [9-11]. Accurate modelling of their propagation in various media is critical to improving system performance across these fields. Furthermore, understanding how different media affect pulse compression and peak power can guide the development of next-generation optical technologies [12-14].

The aim of this paper is to conduct a comprehensive analysis of ultrashort pulse propagation in a silica fiber, air-silica glass, and hollow-core. Through detailed simulations, we examine how dispersion and nonlinear effects shape the pulse characteristics in each medium. We also highlight which optical medium offers the most efficient pulse compression and minimal distortion, providing insights for future applications in advanced photonics.

The remainder of this paper is structured as follows: Section 2 outlines the theoretical background and the derivation of the GNLSE equation. Section 3 describes the simulation setup and parameters. Section 4 presents and discusses the simulation results, and Section 5 concludes with a summary of the findings and potential future work.

2. Theoretical background

Chromatic dispersion can lead to dispersive pulse broadening and pulse compression. For instance, the Kerr effect results in self-phase modulation (SPM) [15-16]. Furthermore, the spatial profile of pulses is shaped not only by linear phenomena-such as diffraction and waveguiding-but also by nonlinear processes like self-focusing. When nonlinear interactions become particularly intense, filamentation can occur, further altering the pulse's spatial characteristics [17-18].

Photonic crystal fibers (PCFs) represent a unique class of optical fibers distinguished from conventional fibers by their specialized structural design, featuring a cladding composed of a periodic array of air holes arranged in a crystal-like lattice. The core is uniquely formed by the deliberate omission of the centermost air hole and/or one or more of the surrounding rings of holes, creating a defect that effectively guides light through the fiber. This network of air holes extends continuously along the entire fiber length, endowing PCFs with exceptional optical properties that conventional fibers do not possess. The emergence of photonic crystals as a research field can be traced back to 1987, when Eli Yablonovitch introduced the concept of photonic bandgap structures. This groundbreaking idea spurred extensive scientific exploration, ultimately paving the way for the development and wide application of photonic crystal fibers [19-21].

When modeling the propagation of ultrashort optical pulses, especially those with broad spectral bandwidths, several critical factors must be considered to accurately capture their behavior. One significant challenge with short optical pulses is that their broad spectral bandwidth can lead to complications. Although the brief pulse duration is advantageous for many applications, the wide range of frequency components makes the pulses more susceptible to dispersion and other effects that can hinder optimal performance. When the spectrum is broad, the variations in absorption across its range become more pronounced. Even if absorption is nearly uniform throughout the pulse's spectral bandwidth, the refractive index still varies with wavelength. This wavelength dependence introduces dispersion effects that ultimately distort the pulse.

The study of nonlinear phenomena in optical fibers advanced significantly due to reductions in fiber loss. This reduction made it possible to observe these nonlinear effects, which required long propagation distances at the power levels. Most research on nonlinear optical effects in fibers was conducted at Bell Laboratories [15, 21-22].

One common way to express light propagation in a lossy, dispersive, and nonlinear fiber is via the generalized nonlinear Schrödinger equation (GNLSE). In a reference frame moving with the pulse-where the retarded time is defined as:

$$\frac{\partial A}{\partial z} + \frac{\alpha}{2}A + \frac{i\beta_2}{2}\frac{\partial^2 A}{\partial t^2} - \frac{\beta_3}{6}\frac{\partial^3 A}{\partial t^3} = i\gamma(|A|^2 A), \quad (1)$$

where:

z : Propagation distance in (meter)

α : Attenuation loss in (dB)

γ : The nonlinear parameter $\gamma = \frac{n_2 w_0}{c A_{eff}}$,

with $n_2 = \frac{3}{8n} Re\left(\chi^{(3)}_{xxxx}\right)$

$\chi^{(3)}_{xxxx}$: Third order susceptibility

β_2 : Second-order dispersion in (ps^2/m)

$A(z,T)$: Pulse envelope.

This equation is often referred to as the Nonlinear Schrödinger (GNLSE) equation when α=0. Attenuation is represented by the first term on the right-hand side of equation (1), while group velocity dispersion (GVD) corresponds to the second term. Nonlinearity, specifically self-phase modulation (SPM), is described by the third term, which depends on intensity.

Equation (1) does not encompass inelastic scattering processes, such as Raman scattering, that become significant when the pulse peak intensity exceeds a certain threshold. Raman scattering involves energy transfer from the optical field to the material's vibrational modes, leading to a delayed nonlinear response. This inelastic process results in phenomena like the Raman self-frequency shift, which can significantly alter the pulse spectrum and temporal shape.

$$P_{cr}^0 \approx 16 \frac{A_{eff}}{L_{eff}\ g_R} \quad (2)$$

A_{eff} is defined in equation (3), L_{eff} effective length, while g_R is the Raman gain.

$$A_{eff} = \frac{\left(\iint_{-\infty}^{+\infty} |F(x,y)|^2 dxdy\right)^2}{\iint_{-\infty}^{+\infty} |F(x,y)|^4 dxdy} \quad (3)$$

If $F(x,y)$ is approximated by a Gaussian distribution, $A_{eff} = \pi r^2$.

When the pulse duration is below 1 ps, the spectral width can be broad enough that Raman gains transfers energy from the higher-frequency components to the lower-frequency components, resulting in a Raman self-frequency shift.

The generalized nonlinear Schrödinger equation (GNLSE) that describes the evolution of the electric field $E(z,T)$ along the propagation direction z is given by:

$$\frac{\partial E(z,T)}{\partial z} = -\frac{\alpha}{2}E - \left[\sum_{m=2}^{4}\frac{i^{m-1}}{m!}\beta_m\frac{\partial^m}{\partial T^m}\right]E + i\gamma\left[|E|^2E + \frac{i}{w_0}\frac{\partial}{\partial T}(|E|^2E) - T_R E\frac{\partial|E|^2}{\partial T}\right] \quad (4)$$

β_m are the coefficients dispersion. We write β as the Taylor expansion.

$$\beta = \beta_0 + \beta_1(w-w_0) + \frac{1}{2!}\beta_2(w-w_0)^2 + \frac{1}{3!}\beta_3(w-w_0)^3 + \cdots + \frac{1}{n!}\beta_n(w-w_0)^n \quad (5)$$

w_0: pulsation.
T_R : Self-frequency shift.
T: The period of propagation.

2.1. Term descriptions

– First term: Loss – accounts for power attenuation due to absorption and scattering.

– Second term: Dispersion – includes higher-order dispersion effects through coefficients β_m.

– Third term: Self-Phase Modulation (SPM) – describes nonlinear phase shifts due to the Kerr effect.

– Fourth term: Self-Steepening – captures the intensity dependence of the group velocity, significant for ultrashort pulses.

– Fifth term: Stimulated Raman Scattering (SRS) – models energy transfer from higher frequencies to lower frequencies through inelastic scattering.

2.2. Split-step Fourier method

The relative speed of this method compared with most finite-difference schemes can be attributed in part to the use of the finite-Fourier-transform (FFT) algorithm. This section describes various numerical techniques used to study the pulse-propagation problem in optical fibers with emphasis on the split-step Fourier method and its modifications [23].

To understand the philosophy behind the split-step Fourier method, it is useful to write Eq. (4) formally in the form

$$\frac{\partial A}{\partial z} = \left(\widetilde{D} + \widetilde{N}\right)A, \quad (6)$$

where $\widehat{D}$ is a differential operator that accounts for dispersion and absorption in a linear medium and $\widehat{N}$ is a nonlinear operator that governs the effect of fiber nonlinearities on pulse propagation. These operators are given by

$$\widehat{D} = -\frac{i\beta_2}{2}\frac{\partial^2}{\partial T^2} + \frac{\beta_3}{6}\frac{\partial^3}{\partial T^3} - \frac{\alpha}{2}, \quad (7)$$

$$\widehat{N} = i\gamma\left(|A|^2 + \frac{i}{w_0}\frac{1}{A}\frac{\partial}{\partial T}(|A|^2A) - T_R\frac{\partial|A|^2}{\partial T}\right), \quad (8)$$

In general, dispersion and nonlinearity act together along the length of the fiber. The split-step Fourier method obtains an approximate solution by assuming that in propagating the optical field over a small distance h, the dispersive and nonlinear effects can be pretended to act independently.

3. Simulation setup and parameters

This section outlines the simulation parameters and methodology used to model the propagation of ultrashort pulses in different optical media [24].

3.1. Simulation environment

The simulations were conducted using a numerical solution of the generalized nonlinear Schrödinger equation (GNLSE) implemented in MATLAB. A split-step Fourier method (SSFM) was used to accurately capture the interplay of dispersion, nonlinearity, and attenuation.

3.2. Initial pulse parameters

The initial input pulse is modeled as a Gaussian pulse without chirp, described by the following equation:

$$E(0,t) = E_0\exp\left(-\frac{t^2}{2\tau_0^2}\right) \quad (9)$$

where:
E_0 is the initial pulse amplitude.
τ_0 is the pulse width (Full Width at Half Maximum, FWHM).

$$T_{FWHM} = 2(ln2)^{1/2}T_0 \approx 1.665T_0 \quad (10)$$

The amplitude at any point z along the fiber is given by:

$$U(z,T) = \frac{T_0}{(T_0^2 - i\beta_2 z)^{1/2}}exp\left(-\frac{T^2}{2(T_0^2 - i\beta_2 z)}\right) \quad (11)$$

Consequently, a Gaussian pulse preserves its shape during propagation, though its width T_1 expands with z as follows:

$$T_1(z) = T_0[1 + (z/L_D)^2]^{1/2} \quad (12)$$

L_D is the dispersion length.

In the context of ultrashort Gaussian pulse propagation through optical fibers, the dispersion length $L_D = \frac{T_0^2}{|\beta_2|}$ is a critical parameter that quantifies the impact of group velocity dispersion (GVD) on pulse broadening.

When ultrashort Gaussian pulses propagate through optical fibers (see Fig.1), the concept of dispersion length

becomes relevant. $L_D = \frac{T_0^2}{|\beta_2|}$ It serves as a vital parameter for measuring the influence of group velocity dispersion (GVD) on the broadening of pulses.

$$U(z,T) = \frac{1}{2\pi}\int_{-\infty}^{\infty} \tilde{U}(0,w) exp\left(\frac{i}{2}\beta_2 w^2 z + \frac{i}{6}\beta_3 w^3 z - iwT\right) dw \quad (13)$$

$U(z,T)$ is the pulse envelope.
w is the angular frequency.

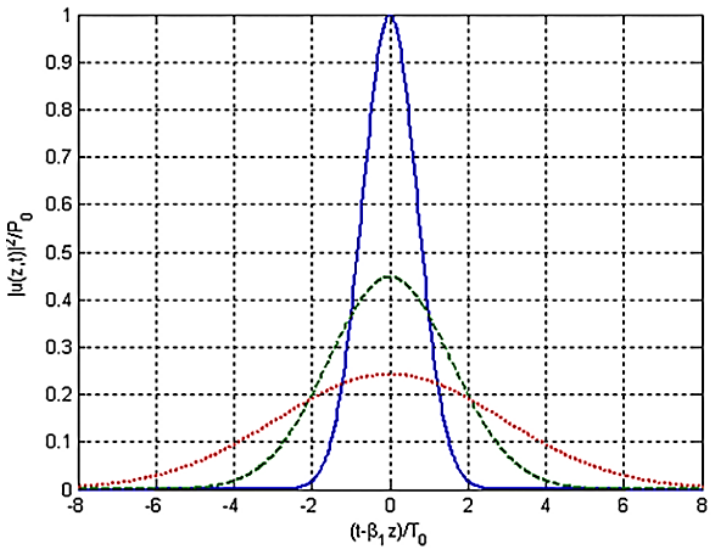

Fig. 1. Dispersion-induced broadening of a Gaussian pulse propagating in a silica fiber is illustrated at $z = 2L_D$ and $z = 4L_D$. The initial pulse profile is depicted by the solid curve at $z = 0$ (colour online)

The third-order dispersion (TOD) effect is given by:

$$L'_D = \frac{T_0^3}{|\beta_3|} \quad (14)$$

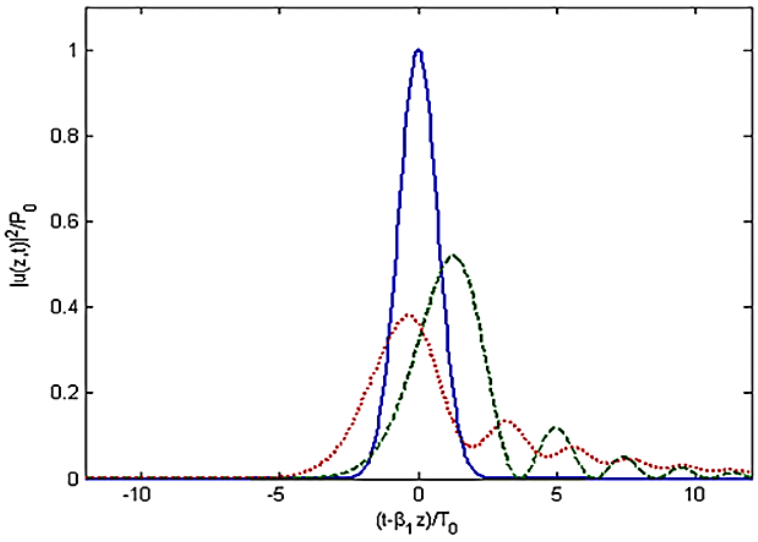

Fig. 2. Pulse profiles at $z = 5L'_D$ for an initially Gaussian pulse launched at $z = 0$ (dotted curve), considering the influence of higher-order dispersion. The dashed curve illustrates the impact of a finite $\beta_2 = 0$ in the case of a silica fiber (colour online)

Ultrashort pulses with durations in the femtosecond range exhibit entirely different dynamics. For instance, third-order dispersion (TOD) can be experimentally investigated by transmitting 100 fs pulses through a fiber that spans several meters (see Fig.2) [21].

While laser pulses are often approximated as Gaussian, other shapes, particularly the hyperbolic-secant profile common in optical solitons and certain mode-locked lasers, warrant consideration. The optical field of these pulses often takes the form [23]:

$$U(0,T) = sech\left(\frac{T}{T_0}\right) exp\left(-\frac{iCT^2}{2T_0^2}\right) \quad (15)$$

Parameter C represents the chirp factor, which determines the initial frequency modulation, or "chirp," of the pulse as it propagates. Its value influences the pulse's temporal and spectral characteristics.

$$T_{FWHM} = 2ln\left(1+\sqrt{2}\right)T_0 \approx 1.763T_0 \quad (16)$$

For instance, the pulse width of a hyperbolic-secant pulse can be related to its FWHM, which differs from that of a Gaussian pulse (see equation (7)).

So, for our simulation we will use the secant hyperbolic pulse. This function is more resistant to broadening than the Gaussian pulse [21-26].

The key pulse parameters are summarized in Table 1:

Table 1. Secant hyperbolic pulse characteristics

Parameter	Value	Parameter	Value
Fiber distance (L)	2 m	Central wavelength (λ)	1060 nm
Gain	1 m		
Mode Field Diameter (MFD)	10 μm	Chirp	0 fs²
Saturation Energy (Esat)	23.56 μJ	Double pulse separation	4 ps

4. Results and discussion

In this section, we present the results of our simulations and discuss the effects of dispersion and nonlinearity on ultrashort pulse propagation in four different optical media: Silica fiber, photonic crystal fiber (PCF), air-silica and hollow-core fiber. We use the hyperbolic-secant profile represented in Fig. 3. In Fig. 3(a) we present the two initial pulses separated by 4 ps. Fig. 3(b) we present the spectrum pulse, Fig. 3(c) we present the autocorrelation function, and in Fig. 4 we present the spectrogram.

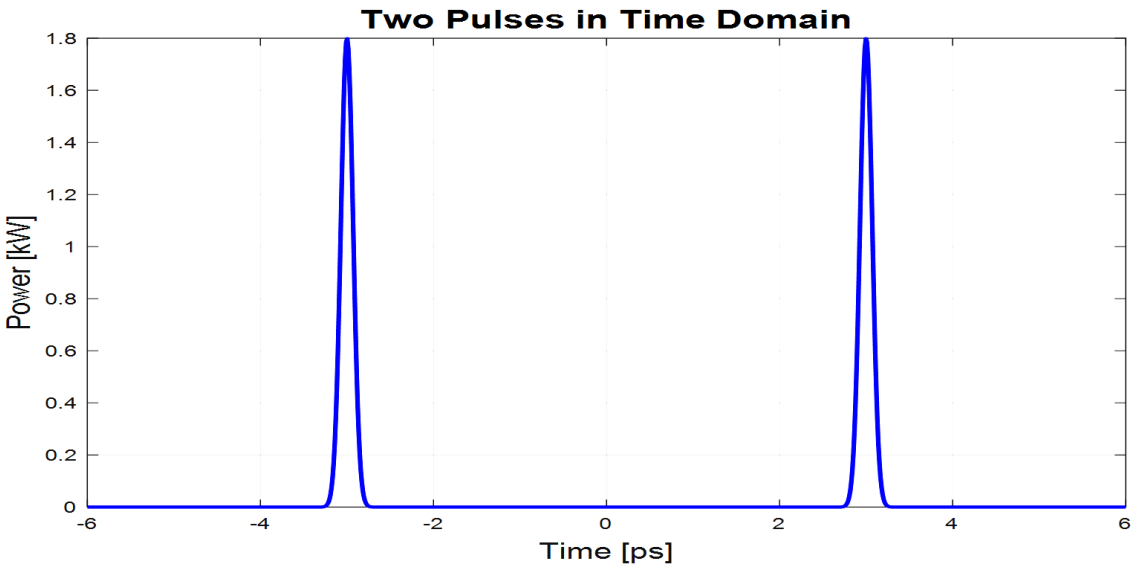

(a)

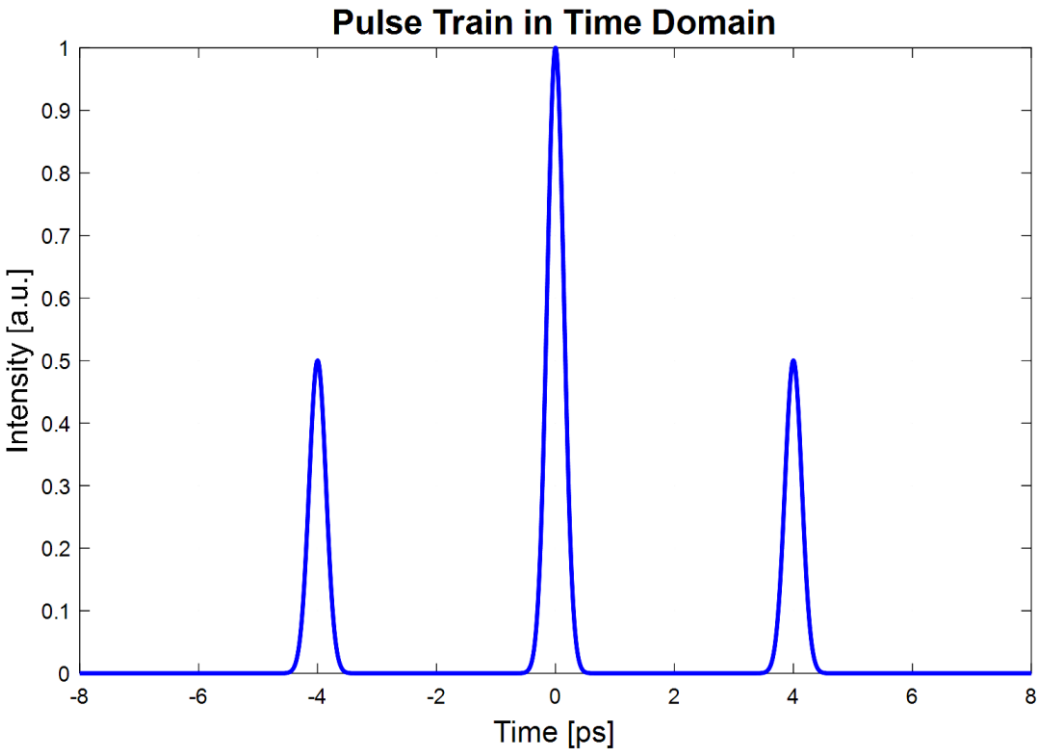

(b)

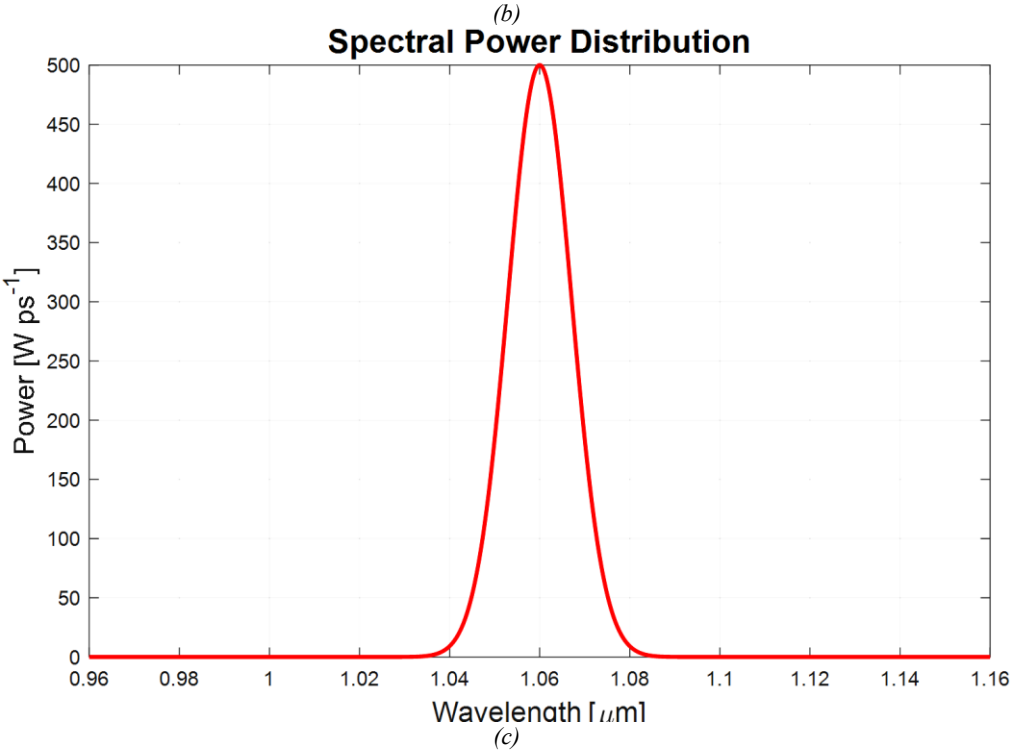

(c)

Fig. 3. (a) Initial pulse profiles at $z = 0$ m, (b) Corresponding autocorrelation function, (c) Spectral representation of the pulse (colour online)

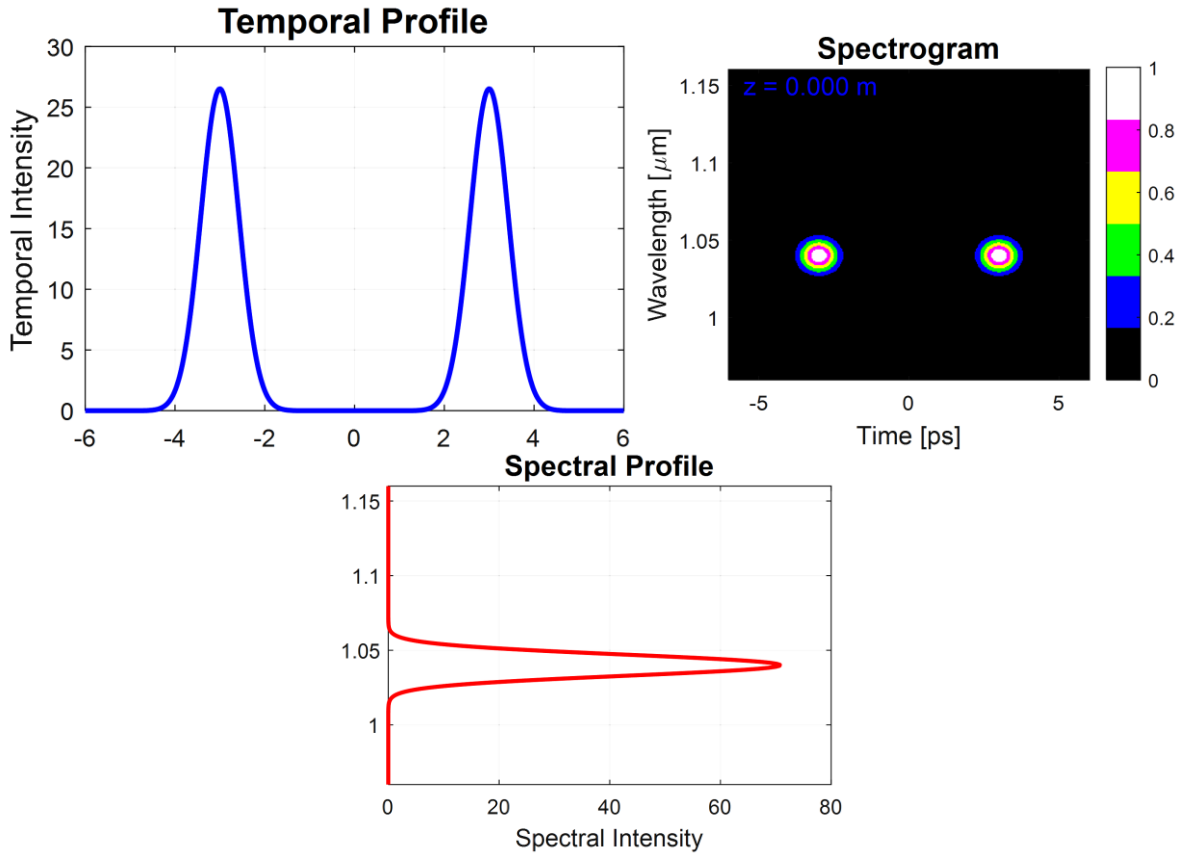

Fig. 4. Spectrogram time-wavelength (colour online)

4.1. Silica fiber (SiO_2)

After passing through amorphous Silica fiber, the pulse displays marked temporal expansion and a drop in peak power.

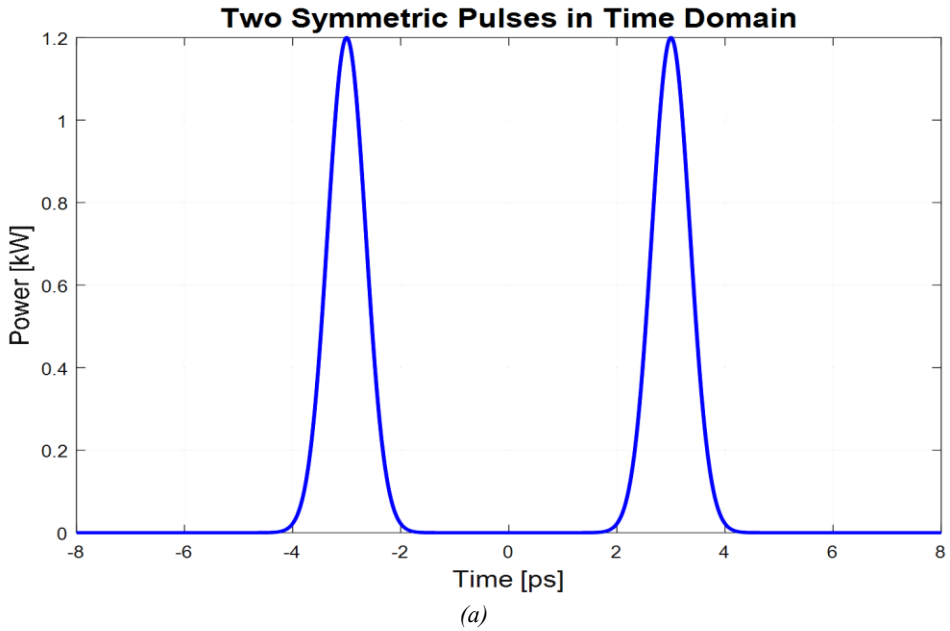

(a)

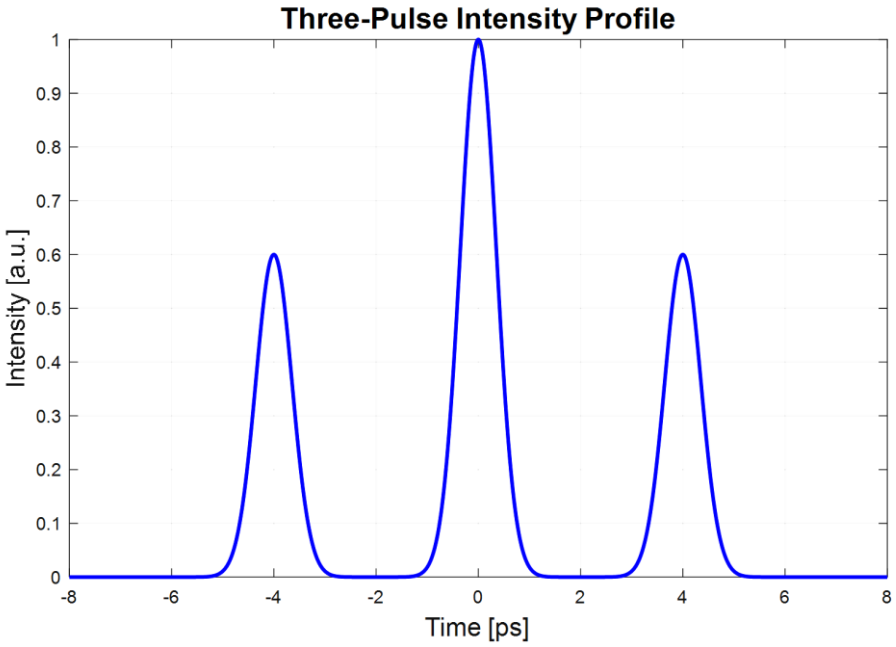

(b)

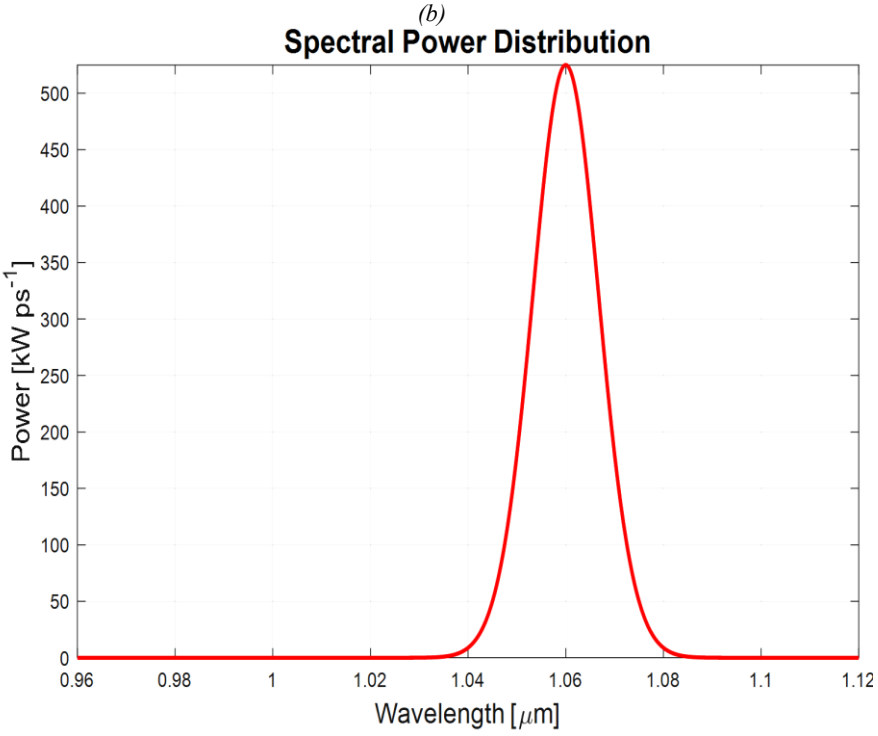

(c)

Fig. 5. (a) Pulse after propagation inside silica fiber $z = 2\ m$, (b) Corresponding autocorrelation function, (c) Spectral representation of the pulse (colour online)

Fig. 5(A) shows the temporal profile of the propagated pulse, while Fig. 5(B) presents the corresponding autocorrelation function, which reveals an increase in pulse duration by 6.02 ps. The pulse's energy decreases to 4.92 nJ, as indicated in Table 5. The spectral broadening observed in Fig. 5(C) is approximately three times larger than the initial pulse, highlighting the influence of self-phase modulation (SPM) and cross-phase modulation (XPM). The pulse power reaches 32.8 MW, contributing to these nonlinear effects.

The wavelength-time spectrogram in Fig. 6 indicates a clear relationship between temporal and spectral components due to chromatic dispersion. Table 2 summarizes the dispersion parameters, highlighting the contribution of higher-order dispersion to pulse broadening and temporal spreading.

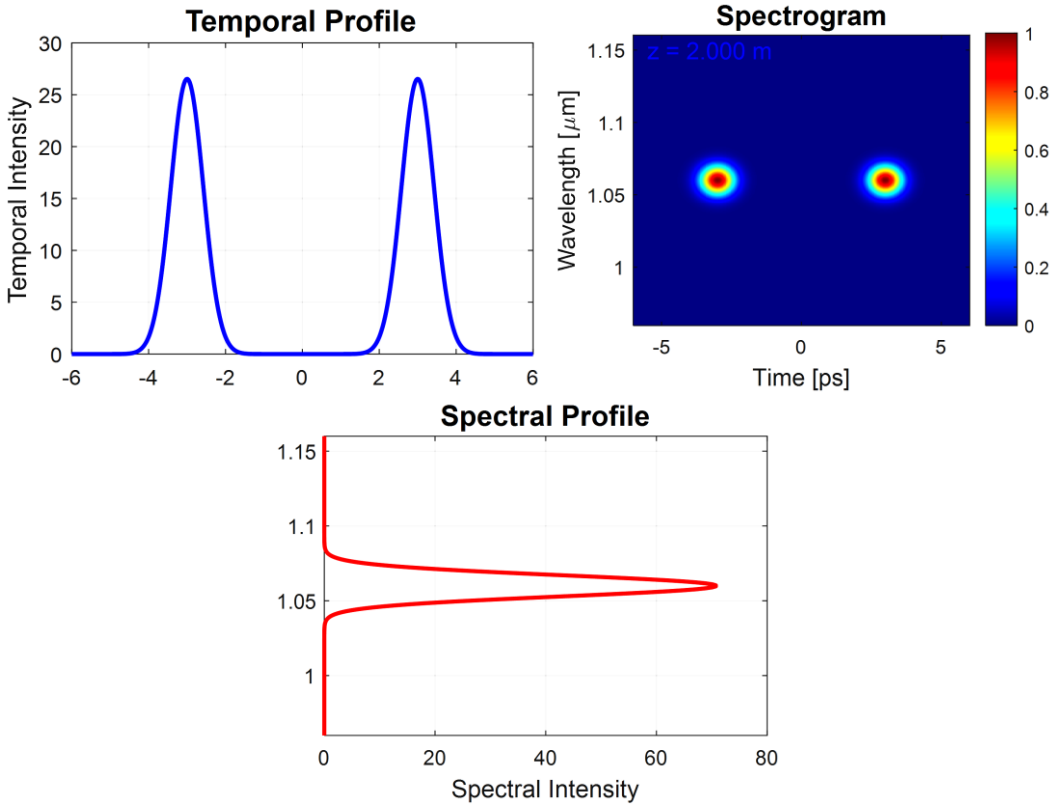

Fig. 6. Spectrogram time-wavelength (silica fiber medium) (colour online)

Table 2. Parameters dispersion results

Dispersion parameters	Value	Dispersion parameters	Value
$\boldsymbol{\beta_2}$	*0.0164 (ps^2/m)*	β_6	*-6.7847 (ps^6/m)*
$\boldsymbol{\beta_3}$	*4.4275 (ps^3/m)*	β_7	*2.11068 (ps^7/m)*
$\boldsymbol{\beta_4}$	*-6.1168 (ps^4/m)*	*Dispersion D*	*-27.499 (ps/(nm.km)*
$\boldsymbol{\beta_5}$	*2.0099 (ps^5/m)*	*Slope S*	*0.1763 ($ps/(nm^2.km)$*

Ps^n/m is the β_m term, where $\beta_m \equiv d^m\beta/d\omega^m$ represents the m-th order dispersion coefficients (see equation 5), D is the coefficient of dispersion, where:

$D = -\frac{2\pi c}{\lambda^2}\beta_2$ [ps/(nm^2. represent km]

S is a slope, where $S = \frac{dD}{d\lambda}$ [ps/(nm^2.km)]

When higher-order dispersion is taken into account, the pulse not only undergoes temporal broadening but also develops asymmetry, with the off-axis regions of the pulse exhibiting a larger temporal width compared to the on-axis component.

$$= (-1)^n 2.\pi.z\left[\frac{\lambda}{2.\pi.c}\right]^n \begin{bmatrix} 1 & 0 & 0 & 0 & 0 \\ 3 & 1 & 0 & 0 & 0 \\ 12 & 8 & 1 & 0 & 0 \\ 60 & 60 & 15 & 1 & 0 \\ 360 & 480 & 180 & 24 & 1 \end{bmatrix} \begin{bmatrix} \emptyset^{(2)} \\ \emptyset^{(3)} \\ \emptyset^{(4)} \\ \emptyset^{(5)} \\ \emptyset^{(6)} \end{bmatrix} \quad (16)$$

We can encode the Taylor expansion up to order n in a matrix [A], which compactly captures all the relevant terms A_{ij}.

$$\emptyset\,(w) = \emptyset(w_0) + (w - w_0)\emptyset^{(1)} + \sum_{i=2}^{p} \frac{1}{i!}(w - w_0)^i\,\emptyset^{(i)}\big|_{w=w_0} + \theta(w) \tag{17}$$

$$\emptyset^{(p)} = (-1)^p . 2\pi . z \left[\frac{\lambda}{2.\pi.c}\right]^p \sum_{j=2}^{p} \lambda^{j-1} A(p-1, j-1) n^{(j)} \tag{18}$$

with $p > 2$.

The propagation effects, including spectral shifts, pulse broadening, and asymmetric distortion in dispersive media, observed both analytically and experimentally, are accurately replicated in our numerical simulations using the proposed formalism. Furthermore, this method enables the analysis of pulses with arbitrary temporal profiles without adding algorithmic complexity. Importantly, unlike analytical approaches, our numerical framework readily accounts for higher-order dispersion effects

4.2. Photonic crystal fiber (PCF)

Pulse propagation in photonic crystal fiber shows moderate improvement over silica fiber. Fig. 7(a) displays the temporal profile, where the pulse broadens to 5.104 ps, indicating less dispersion than fused silica.The autocorrelation function in Fig. 7(b) reflects a more compressed shape, while the spectrum in Fig. 7(c) expands to 11.73 THz, exceeding the spectral broadening observed in a silica fiber.

The pulse peak power reaches 2.28 kW, and a temporal pulse shift of 22.65 fs is observed compared to silica fiber (see Table 5). The wavelength-time spectrogram in Fig. 8 confirms pulse compression with a broader wavelength range than fused silica.

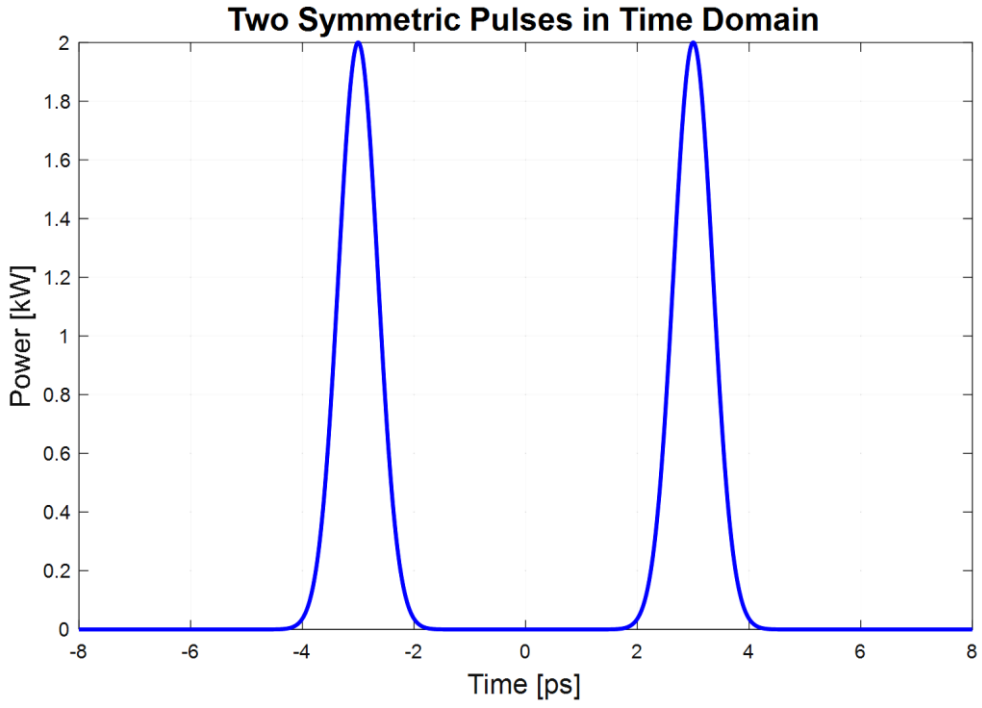

(a)

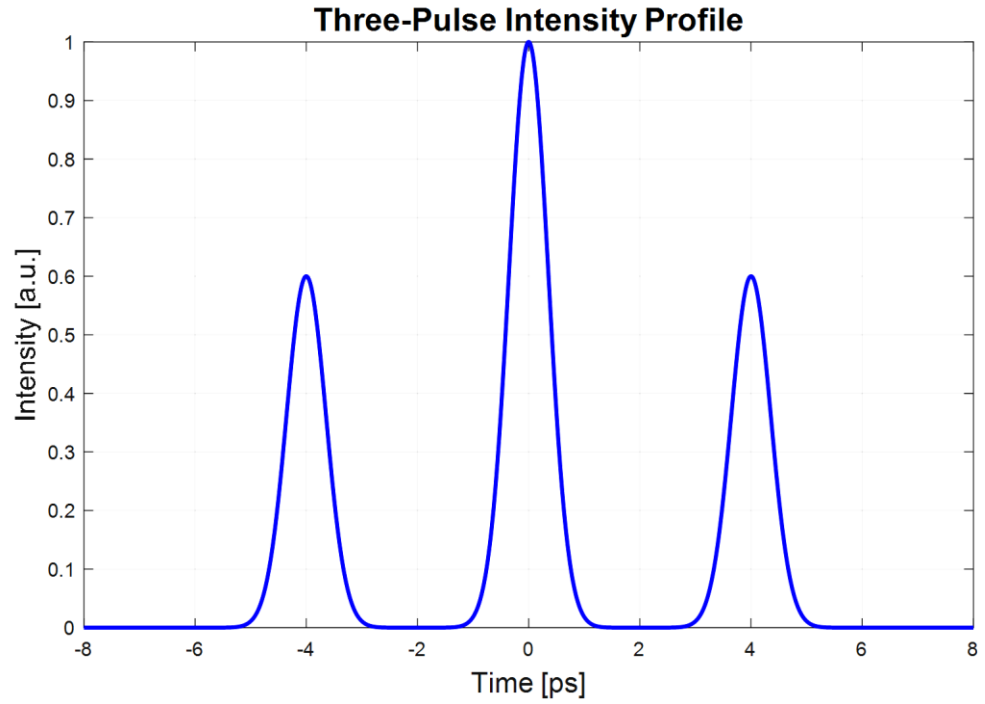

(b)

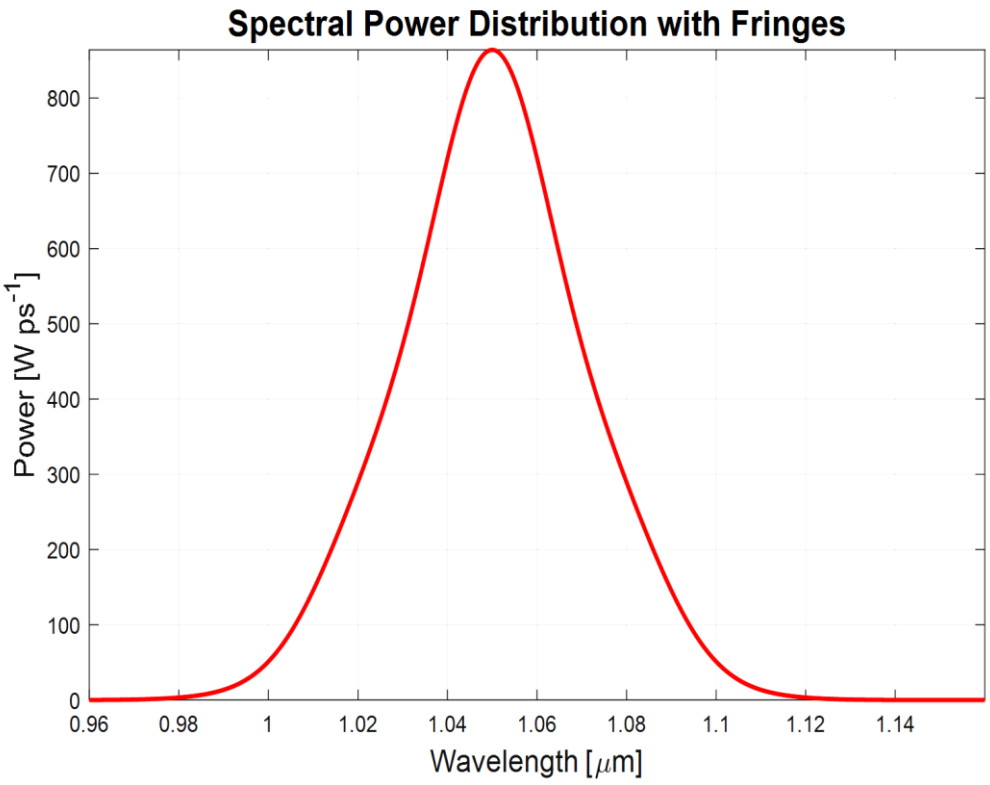

(c)

Fig. 7. (a) Initial pulse profiles at $z = 0$ m, (b) Corresponding autocorrelation function, (c) Spectral representation of the pulse (colour online)

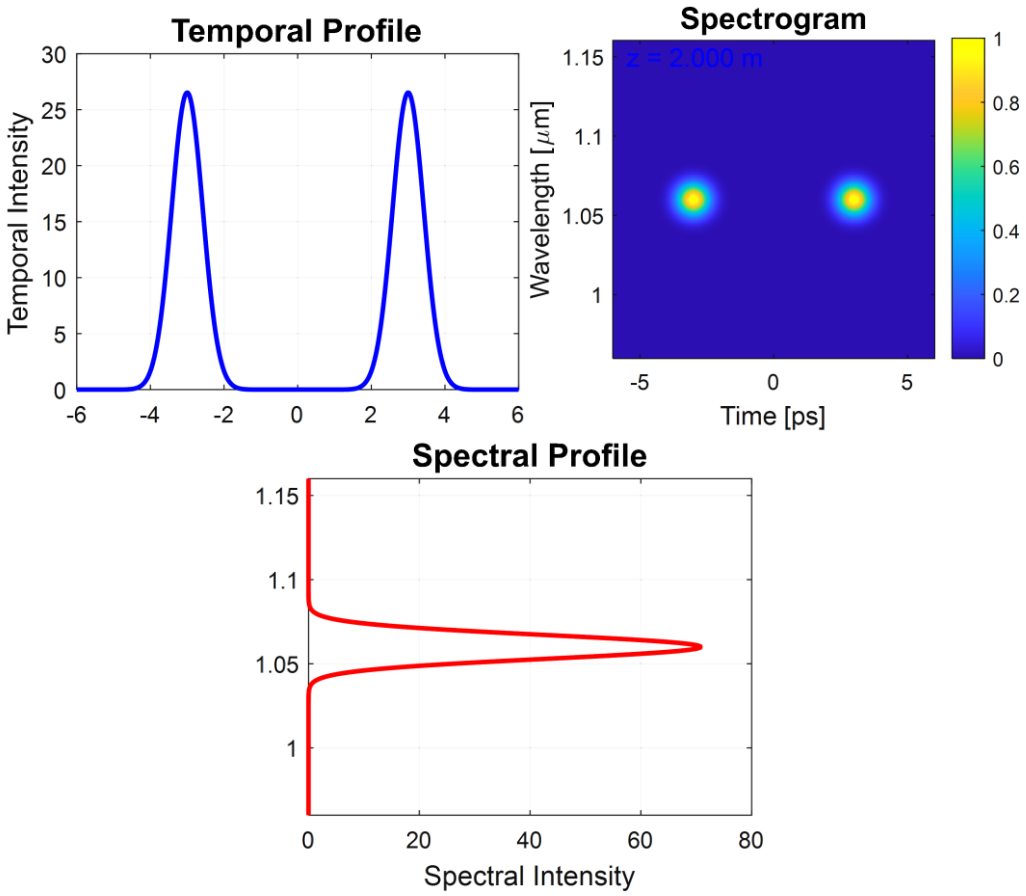

Fig. 8. Spectrogram time-wavelength (photonic crystal fiber) (colour online)

4.3. Hollow-core fiber

Hollow-core fibers demonstrate superior performance in maintaining pulse integrity.

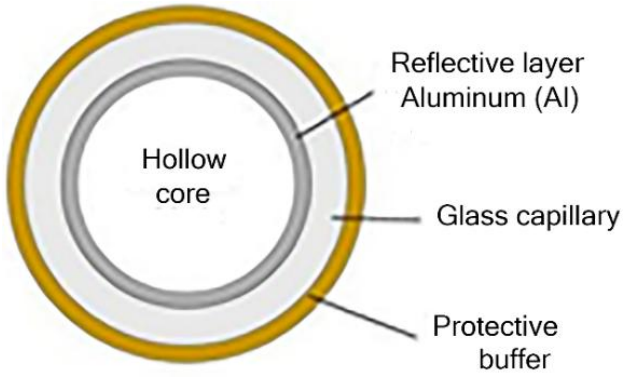

Fig. 9. Hollow-core fiber (colour online)

Fig. 9 illustrates the structural design of the hollow-core fiber. The hollow-core configuration significantly reduces material interaction, resulting in lower nonlinearity and minimal dispersion. This makes hollow-core fibers ideal for maintaining the integrity of ultrashort pulses over long distances.

Fig. 10(a) shows that the pulse compresses to 4.03 ps, exhibiting minimal broadening. The autocorrelation function in Fig. 10(b) indicates a narrow temporal width of 45.71 fs, the lowest among the four materials.

The pulse spectrum in Fig. 10(c) is 4.04 THz, and the peak power reaches an impressive 69.05 kW, significantly higher than other materials. The pulse shift is -0.056 fs (see Table 5), further confirming the superior pulse integrity in hollow-core fibers. The wavelength-time spectrogram likely illustrates the relationship between the wavelength of the pulse and its temporal characteristics. Such a spectrogram can provide insights into how different frequency components of the pulse evolve over time, highlighting dispersion effects and the overall dynamics of pulse propagation.

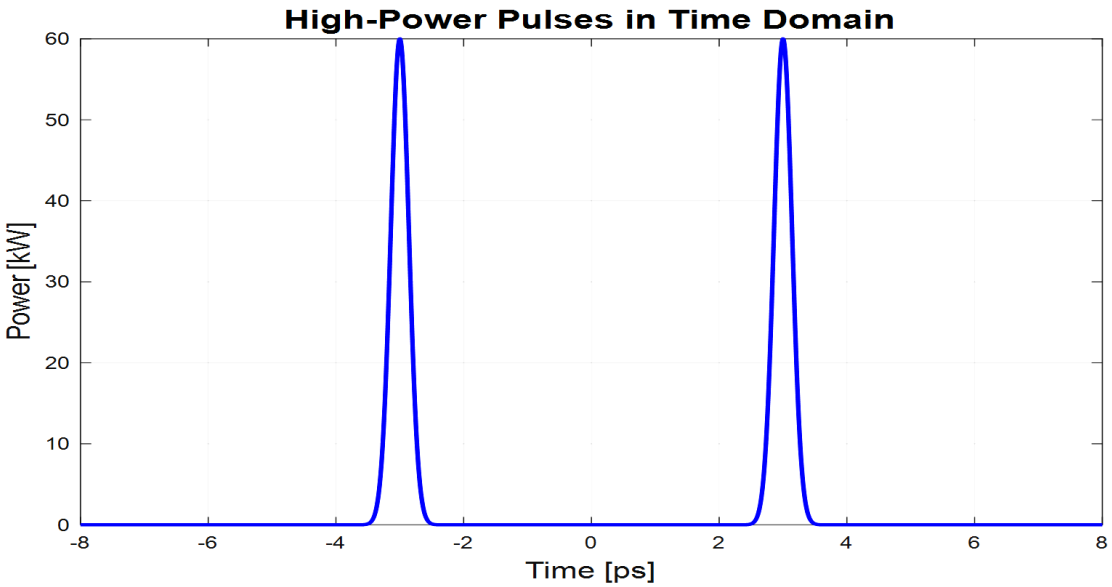
High-Power Pulses in Time Domain
Power [kW]
Time [ps]
60
50
40
30
20
10
0
-8
-6
-4
-2
0
2
4
6
8

(a)

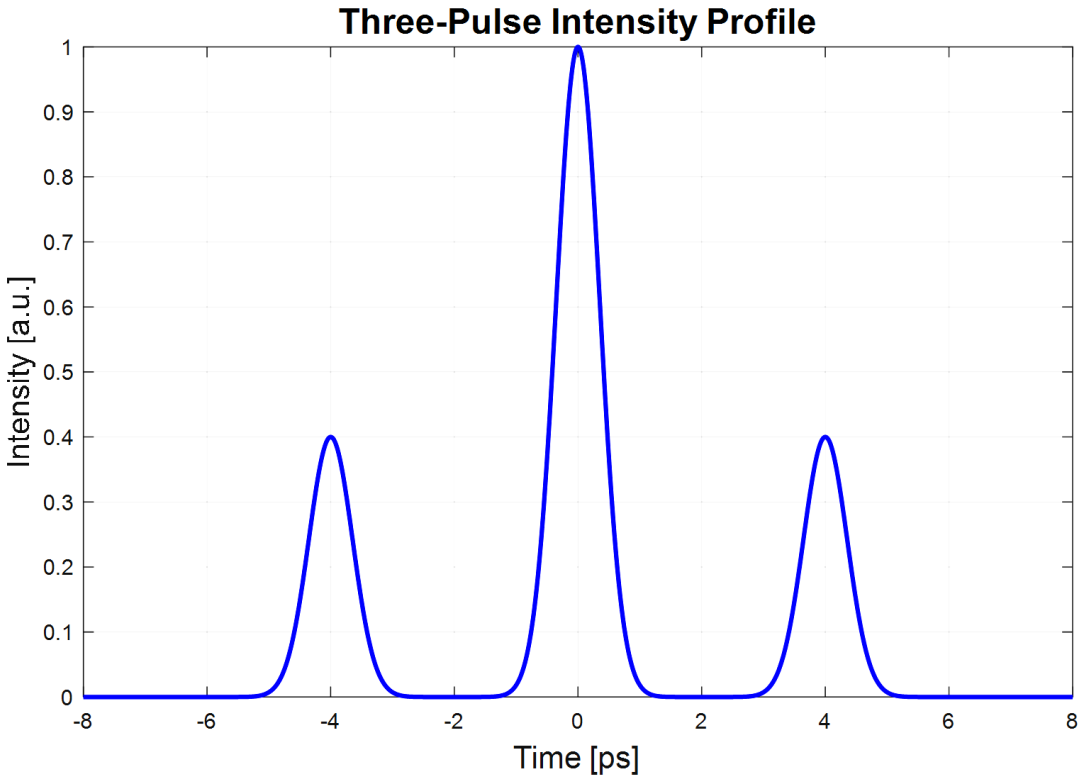
Three-Pulse Intensity Profile
Intensity [a.u.]
Time [ps]
1
0.9
0.8
0.7
0.6
0.5
0.4
0.3
0.2
0.1
0
-8
-6
-4
-2
0
2
4
6
8

(b)

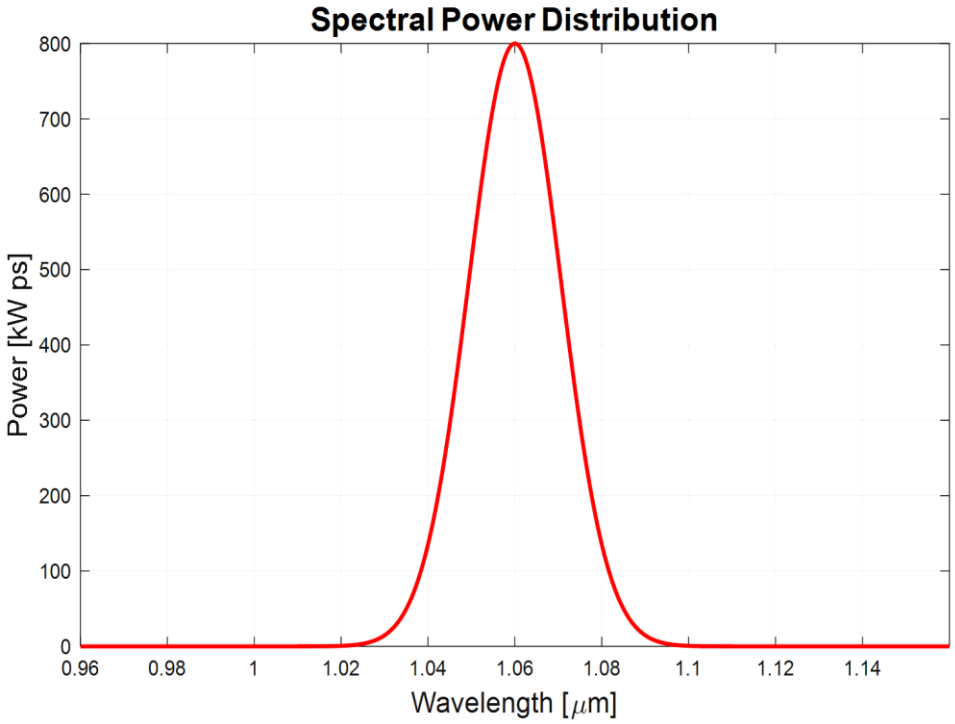

(c)

Fig. 10. (a) Initial pulse profiles at $z = 0$ m, (b) Corresponding autocorrelation function, (c) Spectral representation of the pulse (colour online)

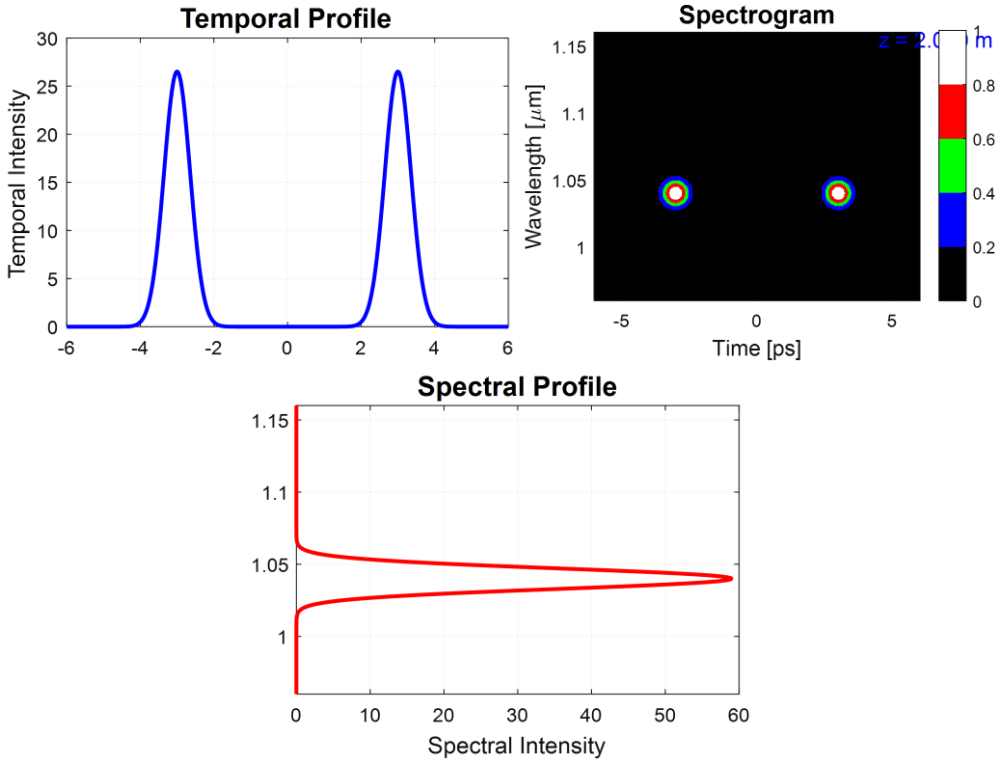

Fig. 11. Spectrogram time-wavelength (hollow-core fiber) (colour online)

Fig. 11 demonstrates efficient confinement with an extensive wavelength range of 1-1.14 µm, comparable to air silica. Table 3 lists the dispersion parameters, highlighting the minimal impact of higher-order dispersion.

Table 3. Dispersion parameters results

Dispersion parameters	Value	Dispersion parameters	Value
β_2	*-0.03905 (ps^2/m)*	β_6	*$5.42e^{-10}(ps^6/m)$*
β_3	*0.00052 (ps^3/m)*	β_7	*$-4.59e^{-10}$ (ps^7/m)*
β_4	*$4.21\ e^{-6}(ps^4/m)$*	***Dispersion D***	*69.3341(ps/(nm.km)*
β_5	*$4.00\ e^{-7}(ps^5/m)$*	***Slope S***	*1.50465(ps/(nm^2.km)*

4.4. Air-silica fiber

Air-silica fibers also exhibit excellent pulse compression capabilities. Fig. 12 presents the structural model of the air silica fiber. The design of the air-filled core effectively reduces dispersion and enhances pulse compression. This fiber type offers superior pulse integrity and minimal distortion, making it suitable for ultrashort pulse propagation in high-speed optical systems.

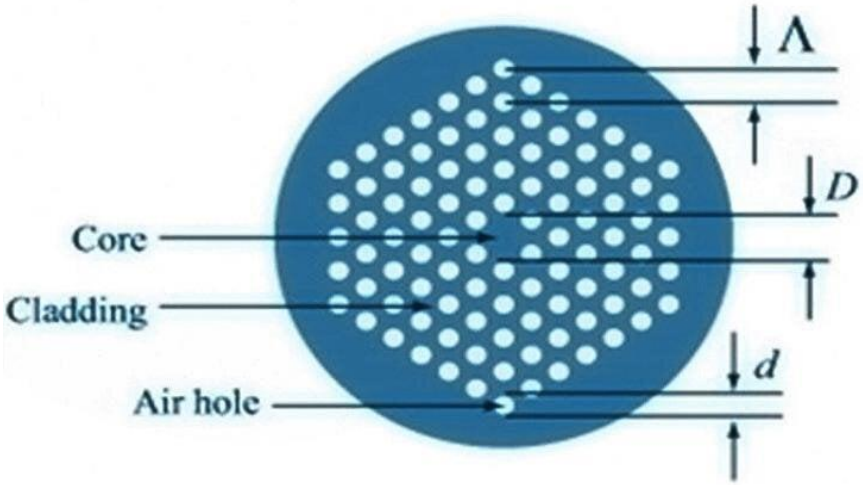

Fig. 12. Air-silica fiber model (colour online)

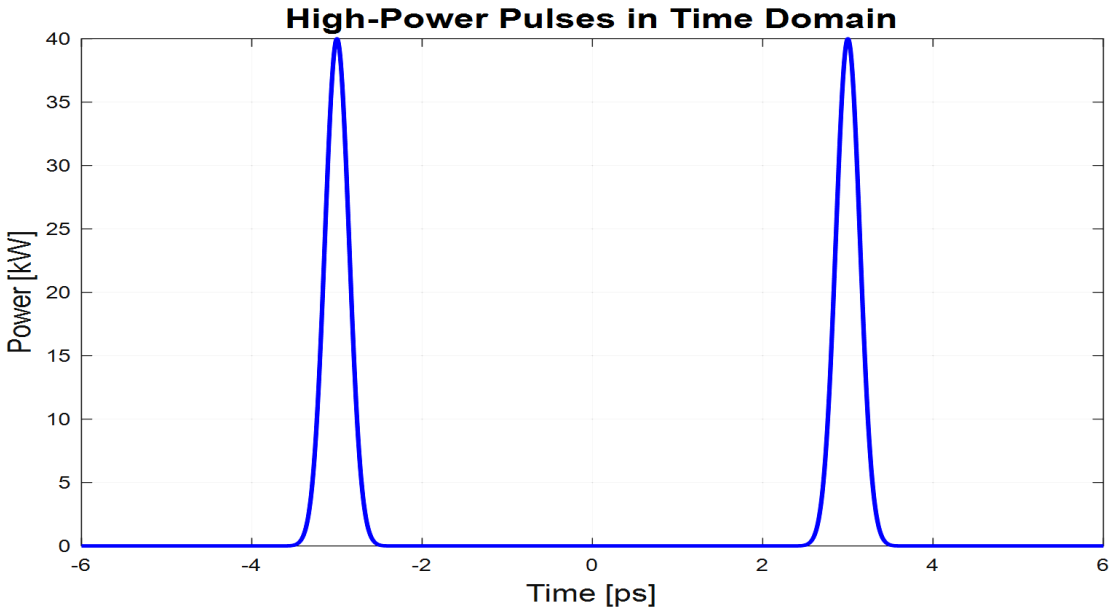

(a)

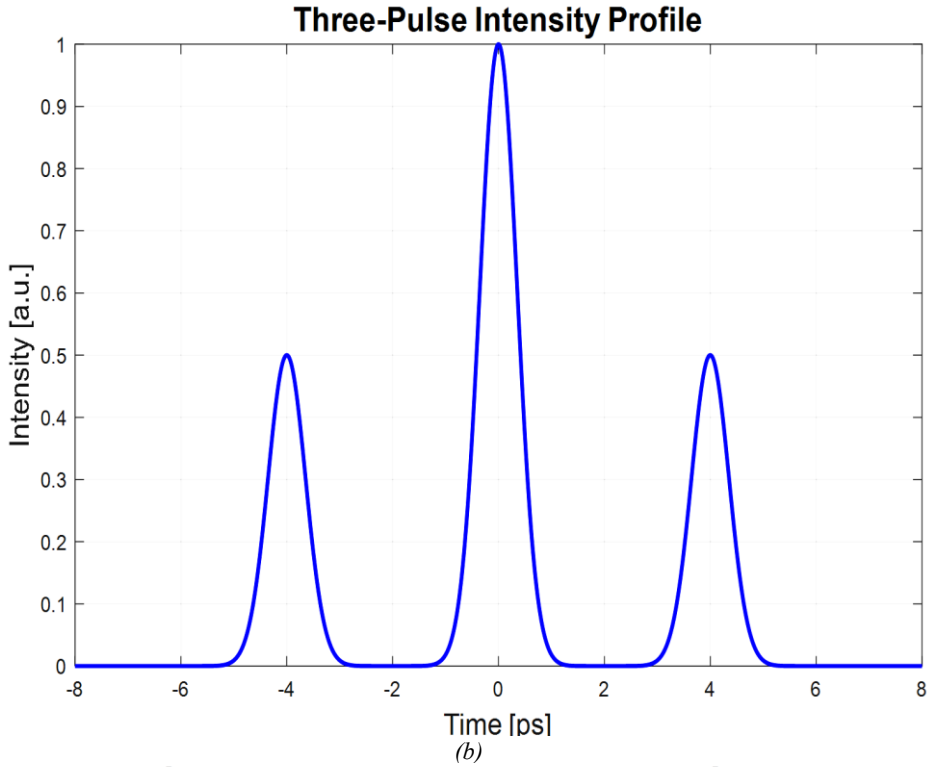

(b)

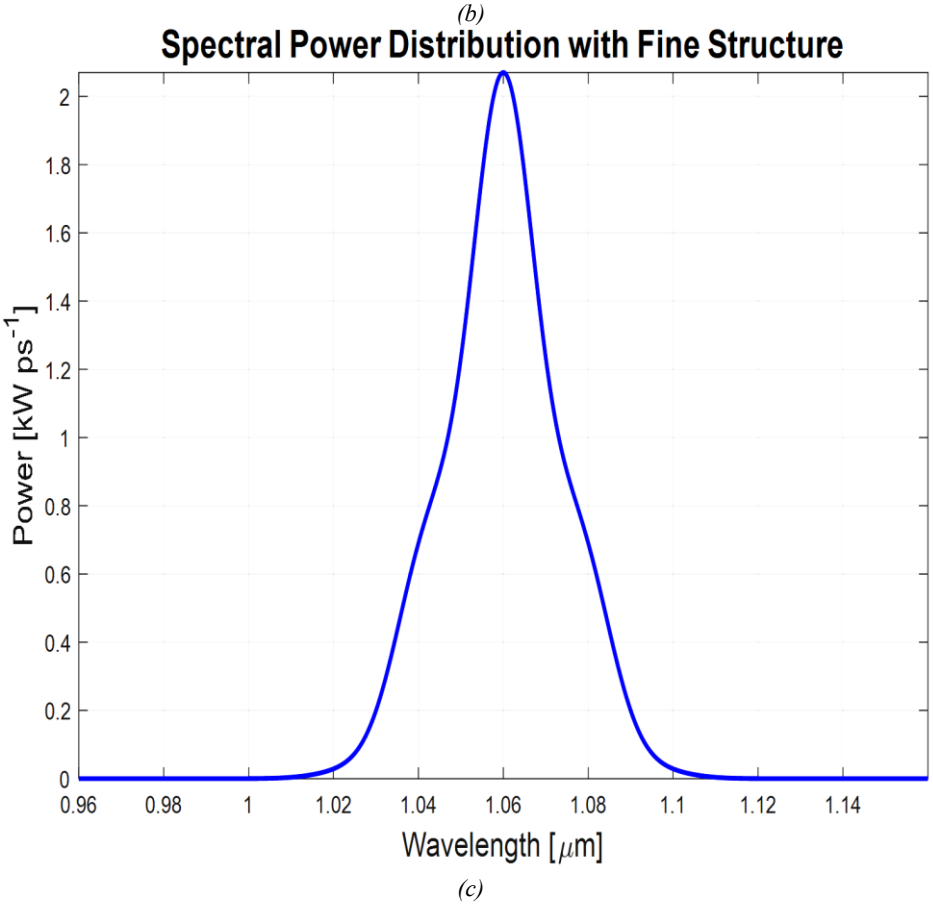

(c)

Fig. 13. (A) Initial pulse profiles at $z = 0$ m, (B) Corresponding autocorrelation function, (C) Spectral representation of the pulse (colour online)

Air-silica fibers also exhibit excellent pulse compression capabilities. Fig. 13(A) shows that the pulse compresses to 4.04 ps, which is comparable to hollow-core fibers. The spectrum in Fig. 13(C) remains relatively unchanged at 5.02 THz, with less spectral broadening than PCF.

The autocorrelation function in Fig. 13(B) reveals two secondary peaks alongside the main peak, indicating some residual pulse-shaping effects. The pulse peak power reaches 43.07 kW, and the pulse shift is -0.005 fs (see Table 5). The wavelength-time spectrogram in Fig. 14 confirms efficient pulse propagation with a wavelength range of 1–1.12 µm, slightly narrower than hollow-core fibers.

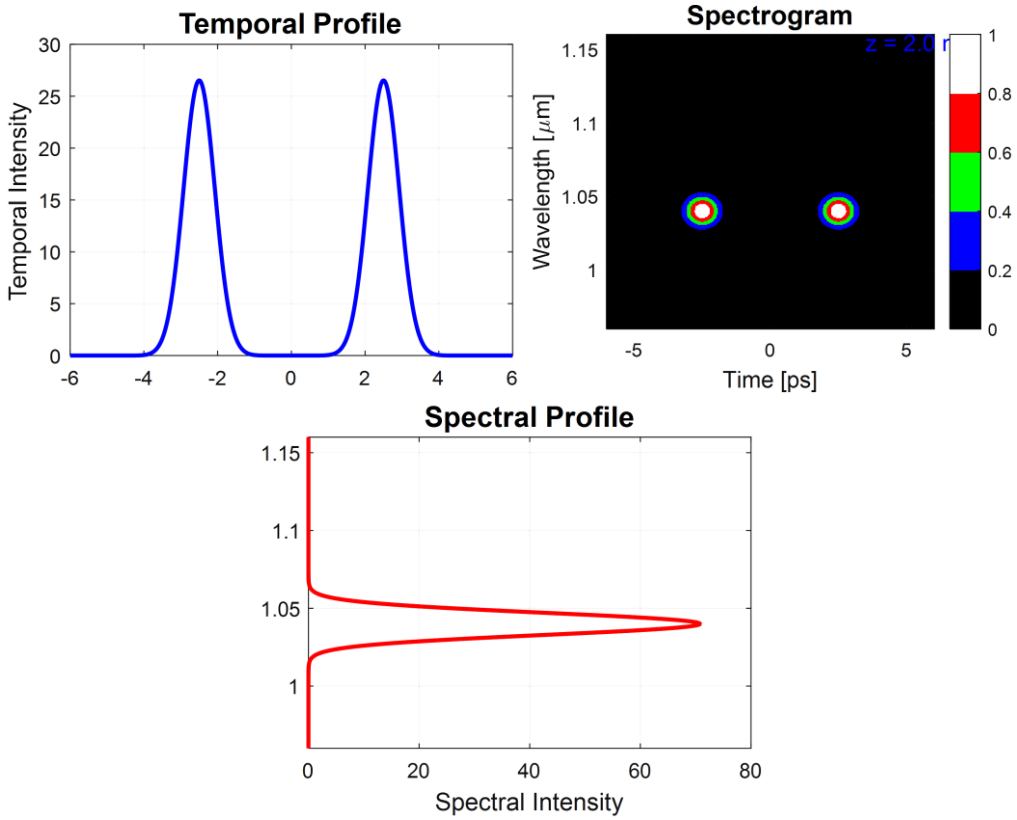

Fig. 14. Spectrogram Time-Wavelength (Air-Silica fiber) (colour online)

Table 4 presents the dispersion parameters, which are comparable to those of hollow-core fibers.

Table 4. Dispersion parameters results

Dispersion parameters	Value	Dispersion parameters	Value
$\boldsymbol{\beta_2}$	*-0.5111 (ps^2/m)*	β_6	*$3.0893e^{-12}$(ps^6/m)*
$\boldsymbol{\beta_3}$	*0.00012 (ps^3/m)*	β_7	*$-2.90e^{-14}$(ps^7/m)*
$\boldsymbol{\beta_4}$	*$-1.19\ e^{-7}$ (ps^4/m)*	*Dispersion D*	*150.4272(ps/(nm.km)*
$\boldsymbol{\beta_5}$	*$3.69e^{-10}$ (ps^5/m)*	*Slope S*	*0.663426 ($ps/(nm^2.km)$*

4.5. Results and analysis

Table 5 provides a comparative overview of key performance metrics across the four media. Advanced porous silica-based fibers exhibit superior pulse compression and peak power performance, positioning them as ideal candidates for ultrashort pulse propagation.

Table 5. Comparative analysis of ultrashort pulse propagation in different materials

parameter	Silica fiber	PCF	Hollow Core	Air Silica
FWHM (ps)	6.02	5.10	4.03	4.04
Spectral FWHM (THz)	7.49	11.73	4.04	5.02
Autocorrelation FWHM (fs)	0.0025	0.0013	45.71	63.12
Peak Power (kW)	1.23	2.28	69.05	43.07
Pulse Shift (fs)	0	22.65	-0.056	-0.005

Silica Fiber: Pulse Width =6.02 Ps and Peak Power = 1.23 KW. Baseline. High nonlinearity (n_2), but also high normal dispersion at common wavelengths. Dispersion spreads the pulse, fighting compression. Poor confinement also leads to loss.

Photonic crystal fiber (PCF): Pulse width = 5.10 ps, and peak power = 2.28Kw. Engineered dispersion. It can be designed for **anomalous dispersion** at visible/NIR wavelengths, enabling compression. Higher confinement increases effective nonlinearity. Better than standard fiber, but still has silica core nonlinearity and loss.

Air-Silica: Pulse width = 4.04 ps, peak power =43.07 Kw. Core is mostly air. Dramatically reduces nonlinearity (n_2_air $\approx$ 0). Why is this good? Because it reduces *unwanted* nonlinear effects (like Raman scattering, self-focusing) that would otherwise steal energy from the pulse peak and distort it. The energy stays in the compressed peak. Also, it can have tailored anomalous dispersion.

Hollow core: Pulse width = 4.04 ps, and peak power = 69.05 Kw. Light propagates >99% in air. Extremely low nonlinearity and ultra-low loss. This is the critical point:

1. Minimal Energy Loss: Less light is absorbed or scattered.

2. Preserved Pulse Shape: No parasitic nonlinearities distort or rob energy from the pulse.

3. Efficient Redistribution: Nearly all the pulse's energy can be funneled into the compressed peak without degradation. The result is a similar compression ratio but a much higher final peak power because the *initial pulse energy is preserved better* throughout the process.

Used silica fiber has a high nonlinearity ($n_2 \sim 2.7\times10^{-20}$ m²/W) that leads to SPM, XPM, and SRS, distorting pulses at high power. Light propagates mostly in air (n_2 of air $\approx 10^{-23}$ m²/W, ~1000× lower than silica). Nonlinear effects (SPM, XPM, SRS) are drastically suppressed, preserving pulse shape and spectrum. Some designs confine light in low-index regions, reducing nonlinearity while maintaining guidance.

Silica fiber damage threshold ~few GW/cm² (limits peak power). Nonlinear effects degrade pulse energy before damage occurs. Higher-order dispersion (β_3, β_4) complicates pulse shaping. On the other hand, Hollow-core fibers have a higher damage threshold (air-core withstands TW/cm² intensities). No nonlinear energy loss → higher peak power transmission.

We showed the pulse compression in HCF, and Air-Silica fibers. Because in anomalous dispersion regimes, some HCFs can introduce negative dispersion ($\beta_2 < 0$), balancing SPM to form solitons or compressed pulses.

Our experimental results confirm that silica fiber induces severe nonlinear and dispersive distortions at high peak powers. At the same time, hollow-core and air-silica fibers mitigate these effects, enabling shorter pulses, higher peak powers, and better spectral fidelity. For applications requiring ultrashort pulse delivery with minimal distortions, these fibers are indeed the superior choice.

From this comparative analysis, it is evident that hollow-core and air-silica fibers are the most suitable materials for maintaining pulse integrity, minimizing dispersion, and maximizing peak power during ultrashort pulse propagation. The pulse width is compressed using a hollow core and the air Silica.

5. Conclusion

This paper investigated the propagation of ultrashort laser pulses in a silica fiber, photonic crystal fiber (PCF), air-silica, and hollow-core fiber. Numerical simulations are performed to analyze pulse evolution under varying input pulse parameters and fiber characteristics. Our focus lied on understanding how these higher-order effects influence pulse broadening, spectral reshaping, and the generation of new frequency components. We specifically examine the interplay between dispersion management and nonlinearity in controlling the output pulse characteristics.

Our simulation results demonstrated that hollow-core and air-silica fibers offer the most effective pulse compression and superior pulse integrity. Specifically, hollow-core fibers achieved the narrowest pulse width of 4.03 ps and the highest peak power of 69.05 kW, making them the most efficient material for ultrashort pulse propagation. Air-silica fibers also performed well, with a compressed pulse width of 4.04 ps and a peak power of 43.07 kW, while maintaining minimal dispersion effects.

Our results further reveal that the combined effects of group velocity dispersion (GVD) and self-phase modulation (SPM) can produce pulses with soliton-like characteristics. Additionally, our analysis indicated that stimulated Raman scattering has negligible effects on pulse propagation in these materials, preserving pulse integrity and energy distribution.

These findings suggest that hollow-core fiber and air-silica fibers are optimal for applications requiring ultrafast optical systems, including high-speed optical communication and ultrafast laser technologies. Future research may explore advanced fiber designs to further improve pulse compression and mitigate nonlinear effects for next-generation photonic applications.

While the analysis provides valuable insights into waveguide performance, its reliance on idealized regimes limits real-world applicability. Key limitations include the neglect of specific loss mechanisms, such as surface scattering and bend loss. Enhancing its rigor will require future work to incorporate these factors into simulations and to pursue experimental validation under realistic fabrication constraints. Nevertheless, the study's strengths, a clear theoretical framework and an innovative methodology, establish a robust foundation for further research.

Data availability

The datasets used and/or analyzed during the current study are available from co-author Pr. Abdelaziz Rabehi (rab_ehi@hotmail.fr) on reasonable request.

Acknowledgements

The researchers wish to extend their sincere gratitude to the Deanship of Scientific Research at the Islamic University of Madinah (KSA) for the support provided to the Post-Publishing Program.

Conflict of interest

The authors declare that they have no conflicts of interest.

References

[1] H.-T. Shang, Electronics Letters **17**(17), 603 (1981).
[2] A. M. Younsi, M. Elbar, A. Rabehi, Semiconductors **58**(12), 984 (2024).
[3] Salah Eddine Boukredine, Elhadi Mehallel, Ahcene Boualleg, Oussama Baitiche, Abdelaziz Rabehi, Mawloud Guermoui, Abdelmalek Douara, Imad Eddine Tibermacine ITEGAM- Journal of Engineering and Technology for Industrial Applications (ITEGAM-JETIA) **11**(51), 65 (2025).
[4] A. D. Pryamikov, A. S. Biriukov, A. F. Kosolapov, V. G. Plotnichenko, S. L. Semjonov, E. M. Dianov, Optics Express **19**(2), 1441 (2011).
[5] H. Han, H. Park, M. Cho, J. Kim, Applied Physics Letters **80**(15), 2634 (2002).
[6] H. A. Haus, J. G. Fujimoto, E. P. Ippen, Journal of the Optical Society of America B **8**(10), 2068 (1991).
[7] A. D. Pryamikov, A. S. Biriukov, A. F. Kosolapov, V. G. Plotnichenko, S. L. Semjonov, E. M. Dianov, Optics Express **19**(2), 1441 (2011).
[8] P. St. J. Russell, Journal of Lightwave Technology **24**(12), 4729 (2006).
[9] P. J. Roberts, F. Couny, H. Sabert, B. J. Mangan, D. P. Williams, L. Farr, M. W. Mason, A. Tomlinson, T. A. Birks, J. C. Knight, P. St. J. Russell, Optics Express **13**(1), 236 (2005).
[10] R. Abdelaziz, D. Abdelmalek, M. Mohamed Elbar, Z. Roumaissa, A. Mohamed, Journal of Engineering and Technology for Industrial Applications (ITEGAM-JETIA) **10**(49), 59 (2024).
[11] A. Douara, A. Rabehi, O. Baitiche, M. Handami, Revista Mexicana de Física **69**(4), 041001 (2023).
[12] A. Rabehi, Revista Mexicana de Física **70**(2), 021004 (2024).
[13] A. Ziane, A. Rabehi, A. Douara, M. Mostefaoui, A. Necaibia, N. Sahouane, R. Dabou, A. Bouraiou, Semiconductors **55**(1), 51 (2021).
[14] A. Rabehi, B. Akkal, M. Amrani, S. Tizi, Z. Benamara, H. Helal, A. Douara, B. Nail, A. Ziane, Semiconductors **55**(4), 446 (2021).
[15] A. Douara, A. Rabehi, M. Guermoui, R. Daha, I. E. Tibermacine, Micro and Nanostructures **195**, 207950 (2024).
[16] R. W. Boyd, Nonlinear Optics, 3rd edition, Academic Press, San Diego, 2008.
[17] N. Bloembergen, Guided Wave Nonlinear Optics, Dordrecht, Springer, Netherlands, 1 (1992).
[18] G. P. Agrawal, Nonlinear Fiber Optics, 4th edition, Academic Press, 2007.
[19] P. P. Mitra, J. B. Stark, Nature **411**(6841), 1027 (2001).
[20] A. M. Younsi, A. Rabehi, L. Gacem, M. T. Soltani, Modern Physics Letters B **38**(9), 2450055 (2024).
[21] O. Baitiche, F. Bendelala, A. Cheknane, A. Rabehi, E. Comini, Crystals **14**(7), 668 (2024).
[22] P. J. Roberts, F. Couny, H. Sabert, B. Mangan, D. Williams, L. Farr, M. Mason, A. Tomlinson, T. Birks, J. Knight, P. St. J. Russell, Optics Express **13**(1), 236 (2005).
[23] G. P. Agrawal, Journal of the Optical Society of America B **28**(12), A1 (2011).
[24] A. Rabehi, M. Amrani, Z. Benamara, B. Akkal, A. Ziane, M. Guermoui, A. Hatem-Kacha, G. Monier, B. Gruzza, L. Bideux, C. Robert-Goumet, Semiconductors **52**(16), 1998 (2018).
[25] B. A. Malomed, Progress in Optics **43**, 71 (2002).
[26] M. W. Bouabdelli, F. Rogti, M. Maache, A. Rabehi, Optik **216**, 164948 (2020).

*Corresponding authors: abdelaziz.rabehi@univ-djelfa.dz
mbenghanem@iu.edu.sa